Article

Discovery Medicine 2026; 38(207): 1274–1290
https://doi.org/10.24976/Discov.Med.202638207.101

GNG4 Promotes Lung Adenocarcinoma Progression by Enhancing mRNA Stability via m6A Methylation to Suppress the cGAS-STING Pathway

Jun Ma[1,2], Jianghong Li[2], Xin Wang[2], Yi Wang[2], Jie Ma[1,*]

[1]Department of Thoracic Surgery, Second Hospital of Shanxi Medical University, 030001 Taiyuan, Shanxi, China
[2]Department of Thoracic Surgery, Heji Hospital Affiliated to Changzhi Medical College, 046000 Changzhi, Shanxi, China
*Correspondence: mjie958@163.com (Jie Ma)
Submitted: 22 January 2026 Revised: 20 March 2026 Accepted: 24 March 2026 Published: 20 April 2026

Background: The malignant progression of lung adenocarcinoma (LUAD) is not only a hallmark of this prevalent cancer but is also closely linked to epigenetic regulation, particularly N6-methyladenosine (m6A) methylation. Disruption of the m6A regulatory machinery results in the uncontrolled upregulation of multiple oncogenic drivers, thereby fueling tumor development. Our study investigated the mechanism by which G Protein Subunit Gamma 4 (*GNG4*), a gene upregulated via m6A modification, promoted LUAD by enhancing its mRNA stability and subsequently inhibiting the cGAS-STING pathway. This provides novel mechanistic insight for clinical LUAD research.

Methods: Based on transcriptomic and m6A sequencing data from The Cancer Genome Atlas Program (TCGA) database, the candidate gene GNG4, associated with m6A regulation, was identified. Correlations of GNG4 expression with two m6A regulators—the writer Vir Like M6A Methyltransferase Associated (VIRMA) and reader Insulin Like Growth Factor 2 MRNA Binding Protein 3 (IGF2BP3)—were statistically evaluated. Prediction of the biological functions pertaining to GNG4 was performed using Single-gene Gene Set Enrichment Analysis (Single-gene GSEA). Cellular experiments, including gene knockdown/overexpression, Western blot, flow cytometry, m6A-related assays, and cellular senescence detection, as well as animal models were employed to investigate the regulatory effects of m6A-modified GNG4 on the cGAS–STING pathway and its impact on cell cycle progression and cellular senescence.

Results: TCGA data combined with functional experiments demonstrated that GNG4 was highly expressed in LUAD ($p < 0.05$). Knockdown of GNG4 activated the cGAS-STING pathway, upregulated p21, induced G1/S cell cycle arrest ($p < 0.05$) and cellular senescence ($p < 0.05$), thereby inhibiting LUAD cell proliferation ($p < 0.05$) and tumor growth ($p < 0.05$). Mechanistically, increased GNG4 mRNA expression was associated with elevated m6A modification in LUAD. GNG4 expression was positively correlated with the m6A writer VIRMA and the m6A reader IGF2BP3. Knockdown of VIRMA or IGF2BP3 significantly reduced both m6A modification and mRNA expression of GNG4 ($p < 0.05$), thereby alleviating its suppressive effect on the cGAS-STING pathway, promoting cellular senescence ($p < 0.05$), and inhibiting proliferation in LUAD cells ($p < 0.05$).

Conclusion: The upregulation of m6A modification of GNG4 in LUAD enhances its mRNA stability, which in turn suppresses the cGAS–STING signaling pathway, ultimately inhibiting cellular senescence and promoting LUAD cell proliferation, thereby driving disease progression.

Keywords: lung adenocarcinoma; m6A methylation; senescence

Introduction

Among all lung cancer diagnoses, approximately 40% are classified as lung adenocarcinoma (LUAD), making it the predominant form of non-small cell lung cancer (NSCLC). This malignancy originates from glandular cells or secretory epithelial cells of the bronchial mucosa and predominantly occurs in the peripheral regions of the lungs [1,2]. While targeted therapy and immunotherapy have led to notable improvements in the diagnosis and management of LUAD [3,4], patient outcomes are still suboptimal. The overall survival rate continues to be unsatisfactory, with particularly grim prognoses for advanced-stage disease [5,6]. Therefore, a more profound understanding of the molecular mechanisms behind LUAD initiation and progression is urgently needed. Concurrently, discovery of novel therapeutic targets remains vital for translating this knowledge into improved clinical outcomes.

The epitranscriptomic modification known as m6A methylation is a critical form of gene regulation that occurs when a methyl group is chemically attached to the sixth nitrogen atom (N6) of adenosine residues in mRNA. This mechanism regulates gene expression by modulating multiple aspects of mRNA, including its half-life, process-

ing, subcellular distribution, and the rate at which it is decoded into protein [7]. Emerging evidence underscores the central involvement of m6A modification in LUAD, influencing disease initiation, progression, metastatic potential and eventual treatment resistance. Dysregulation of m6A regulatory enzymes—writers, erasers, and readers—significantly contributes to malignant progression and holds important clinical prognostic value [8]. Accumulating evidence further points to the dual potential of m6A methylation, along with its interacting lncRNAs, to act as novel biomarkers for both the diagnosis and prognostic assessment of LUAD [9]. Moreover, a higher m6A score in LUAD is closely associated with enhanced tumor invasiveness and the immune infiltration status of the tumor microenvironment [10]. The m6A reader Insulin Like Growth Factor 2 MRNA Binding Protein 3 (IGF2BP3) has been proposed as an independent factor for predicting LUAD prognosis. Its expression shows significant associations with key tumor microenvironment features, including the extent of immune cell infiltration, the levels of immune checkpoint proteins, and the overall tumor mutation burden [11]. Thus, a deeper understanding of the specific regulatory mechanisms by which m6A modification operates in LUAD would advance our knowledge of tumor progression and potentially inform novel immunotherapeutic and targeted treatment strategies.

Functioning within heterotrimeric G proteins, G Protein Subunit Gamma 4 (GNG4) participates broadly in signal transduction. It plays a key role in regulating cellular processes such as proliferation, differentiation, and migration [12,13]. A consistent finding is the heightened expression of GNG4 across diverse malignancies, where its presence is linked to increased malignancy and an unfavorable prognosis [14,15]. Supporting this, emerging research confirms that GNG4 is similarly upregulated in LUAD, a factor strongly linked to adverse clinical outcomes in patients; however, the precise mechanisms through which GNG4 promotes LUAD malignancy remain unclear [16]. A recent study on glioma demonstrated that GNB4 negatively regulates the cGAS-STING pathway [17]. Mechanistically, GNB4, as a Gβ subunit, must form a stable G$\beta\gamma$ dimer with a Gγ subunit (such as GNG4) to exert its signal transduction function [18,19]. This structural characteristic indicates that GNB4's inhibition of the cGAS-STING pathway likely requires G$\beta\gamma$ dimer assembly. Similarly, GNG4 has been implicated in the decline of cognitive functions associated with aging [20], further implying its potential role in cellular senescence and providing a theoretical basis for this study's focus on the mechanism by which GNG4 regulates senescence.

As a core antitumor mechanism, cellular senescence establishes a durable state of cell cycle arrest, a process in which the cGAS-STING pathway plays an indispensable regulatory role [21]. When cells enter senescence due to telomere shortening, oncogene activation, or DNA damage [22], chromatin fragments leak into the cytoplasm and are recognized by cGAS, leading to its activation. As a cytosolic DNA sensor, cGAS initiates downstream cascades and promotes the release of the senescence-associated secretory phenotype [23]. Evidence indicates that the cGAS-STING pathway exerts a dual antitumor effect. On one hand, its activation can induce tumor cell senescence; on the other, it reinforces immune surveillance against these senescent cells, collectively leading to effective tumor suppression.

This study systematically investigated the upregulation of m6A-modified GNG4 and its role in enhancing mRNA stability in LUAD. Furthermore, the study clarified the critical role of the cGAS-STING pathway in GNG4's dual function of suppressing senescence and promoting proliferation. On this basis, the research was designed to identify novel therapeutic targets and elucidate underlying mechanisms, with the aim of informing improved clinical strategies for LUAD.

Materials and Methods

Antibodies and Reagents

The following antibodies and reagents were used: HiFiScript All-in-one RT Master Mix for qPCR (CW3371M, CWBIO), SA-β-Gal Staining Kit (C0602, Beyotime), Human IL-8 enzyme-linked immunosorbent assay (ELISA) Kit (E-EL-H6008, Elabscience), Human IL-6 ELISA Kit (E-EL-H6156, Elabscience), Mouse IL-6 ELISA Kit (CSB-E04639m, CUSABIO), Human Serpin E1/PAI-1 ELISA Kit (E-EL-H2104, Elabscience), cell counting kit-8 (CCK-8) Assay Kit (C0037, Beyotime), Mouse Serpin E1/PAI-1 ELISA Kit (E-EL-M3041, Elabscience), BeyoClick™ EdU Cell Proliferation Kit with AF488 (C0071S, Beyotime), Crystal Violet Staining Solution (C0121-100ml, Beyotime), Anti-cGAS antibody (ab252416, abcam; 0.529 mg/mL, 1:500), Anti-STING antibody (ab288157, abcam; 0.56 mg/mL, 1:500), Anti-Phospho-STING (Ser366) antibody (PA5-105674, Thermo Fisher; 1 mg/mL, 1:500), Anti-NAK/TBK1 antibody (ab40676, abcam; 1.307 mg/mL, 1:500), Anti-NAK/TBK1 (phospho S172) antibody (ab109272, abcam; 0.633 mg/mL, 1:500), Anti-IRF3 antibody (ab68481, abcam; 0.985 mg/mL, 1:500), Anti-IRF3 (phospho S386) antibody (ab76493, abcam; 0.598 mg/mL, 1:500), Anti-p21 antibody (ab109520, abcam; 0.857 mg/mL, 1:500), DAPI Staining Solution (C1006-10ml, Beyotime), Anti-N6-methyladenosine (m6A) antibody (ab284130, abcam; 0.607 mg/mL, 1:500), 5$\times$Loading Buffer (PP117-01, Beyotime), Goat Anti-Rabbit IgG H&L (HRP) (ab7090, abcam; 1 mg/mL, 1:2000), Goat Anti-Mouse IgG H&L (HRP) (ab205719, abcam; 2 mg/mL, 1:2000), Actinomycin D (HY-17559, MCE), BeyoRIP™ RIP Assay Kit (Protein A/G Agarose) (P1801S, Beyotime), Dual Luciferase Reporter Gene Assay Kit (RG027, Beyotime), RNA-Protein Pull Down Kit (NO.B605110, Sangon Biotech), Anti-IMP3 antibody

(ab179807, abcam; 0.11 mg/mL, 1:500), Anti-Ki67 antibody (ab15580, abcam; 1 mg/mL, 1:200), Anti-PCNA antibody (ab29, abcam; 1 mg/mL, 1:200), Anti-Phospho-Histone H3 (Ser10) antibody (66863-1-Ig, proteintech; 1.5 mg/mL, 1:600), Anti-GAPDH antibody (ab181602, abcam; 1.02 mg/mL, 1:1000), Mouse CEA ELISA Kit (CSB-E13925m, CUSABIO), Mouse TK1 ELISA Kit (LS-F19262, Lifespan), Human AFP ELISA Kit (E-EL-M2405, Elabscience), A549 cell complete medium (YM-P-031, UBIGENE), HCC827 cell complete medium (CM-0094, Procell), PMSF (ST507-10ml, Beyotime), phosphatase inhibitor (P1081, Beyotime), RIPA buffer (P0013B, Beyotime), 4% paraformaldehyde (P0099-100ml, Beyotime), 0.1% Triton X-100 (P0096-100ml, Beyotime) , DAPI (C1006-10ml, Beyotime), RNA extraction kit (Vazyme, R711-01), Genious 2×SYBR Green Fast qPCR Mix (Abclonal, RK21207), RU.521 (HY-114180, MCE; 10 μM), and BX795 (HY-10514, MCE; 6 μM).

Cell Culture

In this study, the LUAD cell lines A549 (cat. no. YC-C016, UBIGENE), HCC827 (cat. no. CL-0094, Procell) and the human bronchial epithelial cell line BEAS-2B (CRL-3588, ATCC) were utilized. Cells were authenticated by short tandem repeat (STR) profiling and tested negative for mycoplasma contamination. A549 was cultured in A549 cell complete medium (90%F12K+10%FBS+1%P/S) (YM-P-031, UBIGENE). HCC827 was cultured in HCC827 cell complete medium (RPMI-1640 [PM150110]+10%FBS [164210]+1%P/S [PB180120]) (CM-0094, Procell). BEAS-2B was cultured in RPMI-1640 medium containing 10%FBS, 1%P/S, and 1%sodium pyruvate (C0331, Beyotime). A standard cell culture environment was maintained for both lines, with conditions set at 37 °C and a humidified atmosphere containing 5% carbon dioxide.

Cell Transfection

The Control siRNA, GNG4 siRNA, VIRMA siRNA, IGF2BP3 siRNA sequences are listed below:

Control siRNA: guide 5′-CCUACGCCACCAAUUUCGU-3′;

passenger 5′-ACGAAAUUGGUGGCGUAGG-3′.

GNG4 siRNA: guide 5′-UACAAAAGAACUUCUUCUCGC-3′;

passenger 5′- GCGAGAAGAAGUUCUUUUGUA-3′.

VIRMA siRNA: guide 5′-AGUAUCUAAAAAUAACAGCUC-3′;

passenger 5′-GAGCUGUUAUUUUUAGAUACU -3′.

IGF2BP3 siRNA: guide 5′-AAAAACUACUUUUUGUCUCUU-3′;

passenger 5′-AAGAGACAAAAAGUAGUUUUU-3′.

GNG4 overexpression plasmid (pcDNA3.1-GGamma4-GFP2, #166776) and negative control plasmid (Laconic/pcDNA3.1, #44238) was obtained from Addgene.

Transfection was performed using the SuperKine™ Lipo3.0 Efficient Transfection Reagent (BMU111, Abbkine Scientific Co., Ltd., Wuhan, China). When cells reached 70–80% confluence, the culture medium was replaced with fresh medium prior to transfection. For each transfection setup, two mixtures were prepared in sterile RNase-free tubes: (1) siRNA-Opti-MEM mixture, containing 125 μL Opti-MEM and 5 μL of 20 μM siRNA stock, and (2) transfection reagent-Opti-MEM mixture, consisting of 125 μL Opti-MEM and 6 μL transfection reagent. After gentle mixing, the two solutions were combined, incubated at room temperature for 10–15 minutes, and then applied to the cells.

Western Blotting

To prepare whole-cell lysates, collected samples were treated with ice-cold RIPA lysis buffer (P0013B, Beyotime) containing protease and phosphatase inhibitors (ST507-10ml and P1081, Beyotime) for 30 minutes. Upon centrifugation at 12,000 ×g (15 min, 4 °C), the supernatant was harvested, mixed with 5× SDS sample buffer (PP117-01, Beyotime), and heated at 100 °C for 15 minutes. Proteins were electrophoretically size-fractionated on SDS-polyacrylamide gels and then transferred to Polyvinylidene Fluoride (PVDF) membranes. For immunoblotting, membranes were first blocked with 5% non-fat dry milk in Tris-Buffered Saline with Tween-20 (TBST) for 2 hours at room temperature, followed by an overnight incubation with appropriate primary antibodies at 4 °C. After washing with TBST, blots were incubated with horseradish peroxidase-conjugated secondary antibodies for 2 hours at room temperature, and immunoreactive proteins were visualized with an Enhanced Chemiluminescence detection system (Bio-Rad, USA). Quantitative analysis of band intensity was performed using ImageJ (https://ij.imjoy.io/).

Cell Counting Kit-8 (CCK-8) Assay

Cells were plated in 96-well plates at a density of 5 × 10^3 cells per well and subjected to designated experimental treatments. Following a 24-hour incubation period, 10 μL of CCK-8 reagent (C0037, Beyotime) was introduced to each well, and the plates were then returned to the incubator for an additional 2 hours at 37 °C under light-protected conditions. Subsequently, the optical density at 450 nm was determined using a microplate reader to assess relative cellular viability.

Real-time Quantitative PCR Analysis

We first used an RNA extraction kit (Vazyme, R711-01) for total RNA isolation, followed by reverse transcription with HiFiScript All-in-one RT Master Mix for qPCR (CWBIO, CW3371M). Gene expression levels were quan-

Table 1. Primer sequences used in qRT-PCR analysis.

Gene	Forward sequence	Reverse sequence
GNG4 (human)	5′-GAGGGCATGTCTAATAACAGCAC-3′	5′-AGACCTTGACCCTGTCCATAC-3′
VIRMA (human)	5′-GAGTAAGAGCCCATAGCAGT-3′	5′-TAGCACCAGACCATCAGTATTCAC-3′
IGF2BP3 (human)	5′-TTCAAGGACGCCAAGATCCC-3′	5′-TATCCAGCACCTCCCACTGT-3′
GADPH (human)	5′-CATGAGAAGTATGACAACAGCCT-3′	5′-AGTCCTTCCACGATACCAAAGT-3′

tified by qRT-PCR. Reactions were carried out employing the Genious 2× SYBR Green Fast qPCR Mix (Abclonal, RK21207) according to the manufacturer's instructions. Fluorescence signals were captured in real-time using a compatible qPCR detection system, and cycle threshold (Ct) values were subsequently determined for relative quantification analysis. Glyceraldehyde 3-phosphate dehydrogenase (GAPDH) was used as a normalizer for transcript levels and amplification of individual product was ensured by a melting curve. Primer sequences are shown in Table 1.

Cell Cycle Analysis

For cell cycle distribution analysis, A549 and HCC827 cell lines were cultured in six-well plates to about 80% confluence prior to processing with a commercial Cell Cycle Detection Kit (DA0030, Solarbio). The procedure included fixation in 70% ethanol at 4 °C for 12 hours, incubation with RNase A (100 µL) at 37 °C for 30 minutes, and final staining with PI. Flow cytometric evaluation was then performed as previously described [24].

SA-β-Gal Staining

SA-β-Gal activity was detected according to the commercial kit's instructions (C0602, Beyotime). Briefly, adherent cells were fixed using a 4% formaldehyde solution at room temperature. A freshly prepared staining solution was then added to fully immerse the fixed cell monolayer. For optimal enzyme activity, the staining reaction was carried out in a dry incubator at 37 °C in the absence of CO_2. Following the incubation period, cells were gently rinsed with Phosphate Buffered Saline (PBS) and visualized under a light microscope, as described in the cited methodology [25].

Enzyme-Linked Immunosorbent Assay (ELISA)

ELISA is an immunoassay technique based on the principle of specific antigen-antibody binding. First, a solid surface was coated with a known antibody, followed by the addition of the test sample; if the corresponding antibody was present in the sample, it will bind specifically and become immobilized. An enzyme-linked antibody (AFP, CEA, IL-6, IL-8, PAI-1, TK1) was then added to form an immunocomplex, and finally, an enzyme substrate was introduced for a colorimetric reaction. The target analyte was qualitatively or quantitatively analyzed by measuring the absorbance.

EdU Labeling Assay

Cells were seeded in a 6-well plate and, after overnight recovery, treated accordingly. An equal volume of pre-warmed 2X 5-Ethynyl-2'-deoxyuridine (EdU) solution (20 µM) was added to achieve a final 1X EdU concentration, and the mixture was incubated for 2 hours at 37 °C. The medium was removed and cells were fixed with 4% PFA for 15 min at RT, followed by three washes with buffer. Cells were permeabilized with 0.3% Triton X-100 in PBS for 10–15 min and washed 1–2 times. Then, 0.5 mL Click reaction mixture was added per well, gently shaken, and incubated for 30 min at RT in the dark. After removing the reaction mixture, cells were washed three times and observed under a microscope (ECLIPSE Ts2, Nikon Corporation Healthcare Business Unit). EdU images were analyzed using Image J1 (USA).

Colony Formation Assay

To assess clonogenic potential, cells were seeded at 1×10^3 per well in 6-well plates and maintained under standard conditions for 2 weeks to allow colony formation. Subsequently, cultures were fixed with 4% paraformaldehyde and stained with crystal violet. Colonies (defined as clusters of >50 cells or with a diameter >50 µm) were then manually enumerated or analyzed with dedicated software, and the clonogenic efficiency was derived from these counts. The Colony formation images were analyzed using Image J.

Methylated RNA Immunoprecipitation Combined With Quantitative Polymerase Chain Reaction (MeRIP-qPCR)

RNA extraction was performed with Trizol, followed by RNA immunoprecipitation (RIP) using the BeyoRIP™ Assay Kit (P1801S, Beyotime). Briefly, RNA was fragmented to an average size of 100 nucleotides and then subjected to immunoprecipitation by incubating with an anti-m6A primary antibody (ab284130, abcam) for 2 hours. The antibody-bound RNA complexes were precipitated with Protein A/G Agarose beads. After washing, the enriched GNG4 RNA was reverse-transcribed to generate cDNA, which was then amplified and quantified via qRT-PCR.

m6A Dot Blot Assay

Briefly, RNA was heat-denatured at 95 °C before being transferred onto a membrane and UV-crosslinked. The membrane was then sequentially incubated with an anti-

m6A primary antibody (4 °C) and a corresponding anti-rabbit IgG secondary antibody (room temperature), followed by substrate exposure for signal generation. Dot blot results were recorded under a microscope (OI-X6) for subsequent analysis.

Dual-Luciferase Reporter Assay

The procedure involved cloning the GNG4 3'UTR, in both its wild-type form and with specific m6A site mutations, into the pmiGLO luciferase reporter vector. The resulting plasmids and the pRL-TK plasmid were then co-introduced into the target cells. Following a 48-hour incubation, cells were lysed and assayed with a dual-luciferase detection system. The relative luciferase activity of mutant versus wild-type reporters was calculated from the firefly/Renilla luciferase ratio to assess the regulatory significance of the m6A modification sites.

RNA-Pulldown

To capture the IGF2BP3 protein, biotin-labeled RNA probes corresponding to GNG4 were transcribed *in vitro* and immobilized on streptavidin-coated magnetic beads. The resulting RNA-bead conjugates were incubated with whole-cell lysates to enable specific RNA-protein interaction. Following stringent washes to eliminate nonspecifically bound proteins, the retained complexes were eluted and analyzed by Western blotting. Detection of IGF2BP3 in the eluate confirmed its direct binding to GNG4 mRNA.

Immunohistochemistry

Tissue sections prepared from formalin-fixed, paraffin-embedded (FFPE) blocks were initially deparaffinized and rehydrated, followed by antigen retrieval. After blocking with serum to reduce background staining, sections were incubated overnight at 4 °C with primary antibodies targeting Ki-67, PCNA, and PHH3. Subsequently, after washing with PBS, sections were exposed to HRP-labeled secondary antibodies for 30 minutes at room temperature. Immunoreactivity was visualized using 3,3'-Diaminobenzidine chromogen, and hematoxylin was used as a nuclear counterstain. Thereafter, sections were dehydrated, cleared, mounted with coverslips, and observed under a light microscope. Protein expression was semi-quantitatively assessed by combining the proportion of positively stained cells with the intensity of staining.

Measurement of mRNA Half-Life

To assess the stability and decay kinetics of GNG4 mRNA, we performed a transcriptional inhibition assay followed by time-course analysis. Cells were treated with actinomycin D, a potent inhibitor of RNA polymerase, to completely block de novo RNA synthesis. Following transcriptional arrest, total RNA was harvested at sequential time points (0, 2, 4, and 6 hours). The abundance of the remaining GNG4 transcripts at each time point was then precisely quantified using qRT-PCR. By plotting the relative mRNA levels against time and fitting the data to an exponential decay model, we calculated the half-life of GNG4 mRNA, which represents the time required for a 50% reduction in its steady-state level under these conditions.

Animal Model

To assess the *in vivo* effect of gene silencing on tumor growth, a xenograft model was established using female BALB/c nude mice (age: 6 weeks; weight: 18–22 g; sourced from SiPeiFu Biology Ltd., China). The mice were randomly allocated into three groups (n = 6 per group): a non-targeting siRNA control (si-NC), a GNG4-knockdown group (si-GNG4), and a VIRMA-knockdown group (si-VIRMA). A549 cells (5×10^6 cells/mouse), in which the corresponding genes had been knocked down *in vitro* prior to inoculation, were subcutaneously injected into the right axillary fossa of each mouse. Mice were maintained under standard housing conditions (temperature: 22 ± 2 °C; humidity: 50% ± 10%) with free access to food and water throughout the four-week modeling period. Tumor volumes were measured weekly using the formula: (length × width^2)/2. After four weeks, mice were anesthetized via intraperitoneal injection of pentobarbital sodium (50 mg/kg) and subsequently euthanized by cervical dislocation under deep anesthesia. Blood samples were collected via retro-orbital bleeding, and subcutaneous tumors were excised for further analysis. This study was approved by the Experimental Animal Ethics Committee of Heji Hospital Affiliated to Changzhi Medical College (DW2026003).

Bioinformatics Analysis

Gene expression data for LUAD were downloaded from The Cancer Genome Atlas (TCGA) database (https://portal.gdc.cancer.gov/) (Adjacent normal tissue: n = 59, tumor: n = 530). Differential expression analysis between normal and tumor groups was performed using the "limma" package with thresholds set at |logFC| >1 and adj.*p*.val < 0.05. This analysis identified 4473 differentially expressed genes (DEGs), including 2015 upregulated genes. Similarly, m6A methylation data for LUAD were obtained from the TCGA database (Adjacent normal tissue: n = 32, tumor: n = 471). Differential methylation analysis was conducted using the "ChAMP" package with thresholds of |logFC| >0.4 and FDR <0.05, yielding 863 differentially methylated genes, of which 661 were hypermethylated. The upregulated and downregulated DEGs were separately subjected to Kyoto Encyclopedia of Genes and Genomes (KEGG) pathway and Gene Ontology (GO) term enrichment analyses using the "clusterProfiler" package. Gene expression levels were visualized via box plots generated with "ggplot2", and the Wilcoxon rank-sum test was applied to assess the statistical significance of expression differences. Correlation analysis among genes was performed using the "psych" package. A correlation network

was constructed and visualized with "ggraph", displaying only gene pairs with correlation coefficients >0.4. Correlation heatmaps were generated using "pheatmap". Finally, scatter plots illustrating the most significant correlation between the target gene and m6A readers/writers were created with "ggplot2".

Statistical Analysis

Each experiment was repeated three times, and quantitative data are presented as the mean ± standard deviation (SD). Statistical analyses were performed using GraphPad Prism 8.3.0 (USA). For comparisons between two groups, an unpaired two-tailed Student's *t*-test was applied. For comparisons involving multiple factors, two-way analysis of variance (ANOVA) was conducted, followed by Tukey's multiple comparisons test. A *p*-value of less than 0.05 was considered statistically significant.

Results

GNG4 Is Highly Expressed in LUAD and Promotes LUAD Progression

To elucidate the expression pattern and functional role of GNG4 in lung adenocarcinoma (LUAD), we initiated a systematic investigation integrating computational bioinformatics and *in vitro* validation. Publicly available transcriptomic data from TCGA and Gene Expression Omnibus (GEO) demonstrated a marked elevation of GNG4 mRNA levels in LUAD tissues compared with normal counterparts (Fig. 1A,B, $p < 0.05$). Clinically, elevated GNG4 expression was significantly associated with poor patient outcomes, including prolonged overall survival (OS, $p = 0.015$), disease-specific survival (DSS, $p = 0.008$), and progression-free interval (PFI, $p = 0.006$) (Fig. 1C). To corroborate these database findings at the cellular level, we subsequently quantified GNG4 mRNA expression in the normal bronchial epithelial cell line BEAS-2B and a panel of LUAD cell lines (A549, HCC827). We found GNG4 expression was notably elevated in cancer cells (Fig. 1D, $p < 0.001$), consistent with the database results. After assessing the efficiency of GNG4 knockdown (Fig. 1E, $p < 0.01$), we found that compared to control cells, LUAD cells with GNG4 knockdown exhibited a significant increase in the expression of key senescence-associated secretory phenotype (SASP) components, namely IL-6, IL-8, and PAI-1 (Fig. 1F, $p < 0.0001$). These findings support the conclusion that GNG4 deficiency induces a senescent state. Furthermore, EdU staining experiments (Fig. 1G, $p < 0.05$) and CCK-8 assay (Fig. 1H, $p < 0.01$) consistently demonstrated that GNG4 knockdown markedly suppressed the cell growth vitality of LUAD cells. In summary, GNG4 was upregulated in LUAD and enhanced tumor cell proliferation by suppressing cellular senescence.

GNG4 Suppresses LUAD Cells Senescence and Promotes Its Proliferation by Inhibiting the cGAS-STING Pathway

To elucidate the pathway mediating GNG4's roles in suppressing senescence and enhancing proliferation in LUAD, we examined the cGAS-STING signaling axis. Silencing GNG4 expression in LUAD cells (Fig. 2A, $p < 0.0001$) led to the pronounced activation of this pathway, reflected by elevated levels of cGAS, phosphorylated STING, TBK1, IRF3, and their total protein counterparts, alongside upregulation of the senescence marker p21 (Fig. 2B). To verify whether the functional influence of GNG4 is mediated by its repression of the cGAS-STING pathway, we conducted rescue studies. In cells with GNG4 knockdown, pharmacological inhibitors targeting cGAS (RU.521) or TBK1 phosphorylation (BX795) were introduced. Notably, both inhibitors significantly attenuated the activation of the cGAS-STING signaling cascade that was triggered by GNG4 depletion. More importantly, both inhibitors effectively rescued the phenotypic consequences of GNG4 loss, including G1/S phase cell cycle arrest (Fig. 2C, $p < 0.05$), reduced proliferative capacity (Fig. 2E, $p < 0.05$), and enhanced cellular senescence (Fig. 2D, $p < 0.0001$). Collectively, these results establish that GNG4 inhibits cellular senescence and stimulates proliferation in LUAD cells, operating through a mechanism that involves the repression of the cGAS-STING signaling pathway.

Increased m6A Methylation of GNG4 Enhances Its mRNA Expression in LUAD

To elucidate the regulatory mechanism responsible for GNG4 upregulation in LUAD, we conducted an analysis of m6A methylation patterns. Principal component analysis (PCA) of m6A methylation data from LUAD samples (Fig. 3A) and a volcano plot of differentially methylated genes (Fig. 3B) revealed 59 genes including—GNG4—that exhibited simultaneous significant upregulation in both m6A methylation levels and mRNA expression (Fig. 3C,D,G). At the functional level, Gene Ontology (GO) enrichment analysis showed that the co-upregulated genes were significantly linked to molecular activities including DNA-binding transcription activator function, especially those specific to RNA polymerase II (Fig. 3E). At the pathway level, KEGG analysis suggested these genes are involved in specific biological contexts, such as maturity-onset diabetes of the young and pathways governing stem cell pluripotency (Fig. 3F). To assess whether GNG4 was directly regulated by m6A modification, we performed site prediction using the SRAMP online tool, which identified adenine 2131 as the most probable m6A methylation site within the GNG4 transcript (Fig. 3H). At the level of expression regulation, further correlation assessments identified a significant positive relationship between GNG4 mRNA abundance, the expression levels of the m6A methyltransferase VIRMA and the m6A-binding

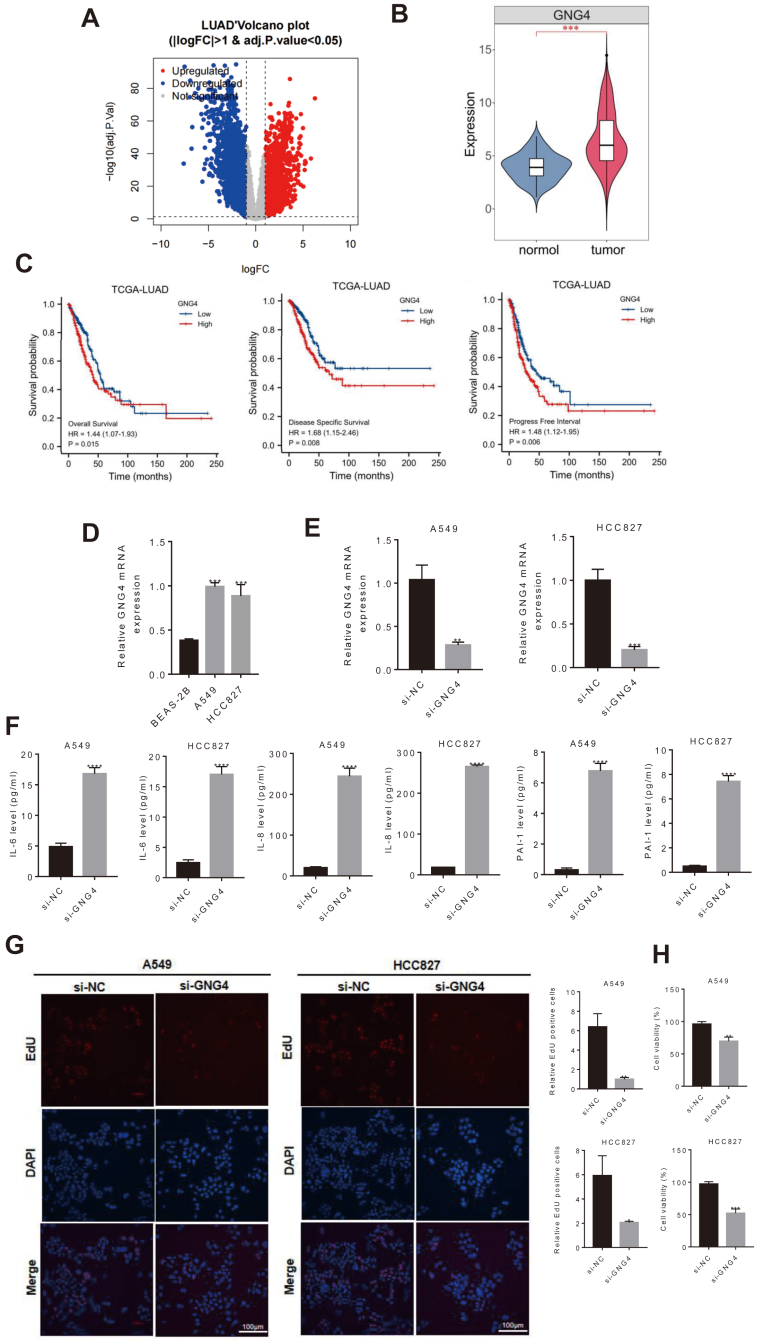

Fig. 1. GNG4 is highly expressed in LUAD and promotes LUAD progression. (A) Volcano plot displaying differentially expressed genes in LUAD based on TCGA-LUDA analysis. (B) Box plot illustrating differential expression of GNG4 in LUAD tissues from the TCGA-LUAD cohort. (C) OS, DSS, and PFI analyses based on GNG4 expression levels in TCGA-LUAD. (D) qRT-PCR analysis of GNG4 mRNA expression in normal bronchial epithelial BEAS-2B cells and LUAD cell lines (A549 and HCC827). (E) qRT-PCR analysis of GNG4 mRNA in A549 and HCC827 after GNG4 knockdown. (F) ELISA measurement of IL-6, IL-8, and PAI-1 secretion in A549 and HCC827 cells following GNG4 knockdown. (G) EdU staining assay evaluating proliferative activity in A549 and HCC827 cells following GNG4 knockdown. (H) CCK-8 assay was used to detect changes in the viability of A549 and HCC827 cells after GNG4 knockdown. mRNA levels are expressed as fold change relative to the vehicle control after normalization to GAPDH. GNG4, G protein subunit gamma 4; LUAD, lung adenocarcinoma; TCGA, The Cancer Genome Atlas Program; OS, overall survival; DSS, disease-specific survival; PFI, progression-free interval; ELISA, enzyme-linked immunosorbent assay; IL, Interleukin; PAI, Plasminogen Activator Inhibitor; EdU, 5-Ethynyl-2'-deoxyuridine; CCK-8, cell counting kit-8; GAPDH, glyceraldehyde 3-phosphate dehydrogenase; NC, negative control. *$p < 0.05$ vs. si-NC group; $p < 0.05$ was considered statistically significant. *$p < 0.05$, **$p < 0.01$, ***$p < 0.001$, ****$p < 0.0001$.

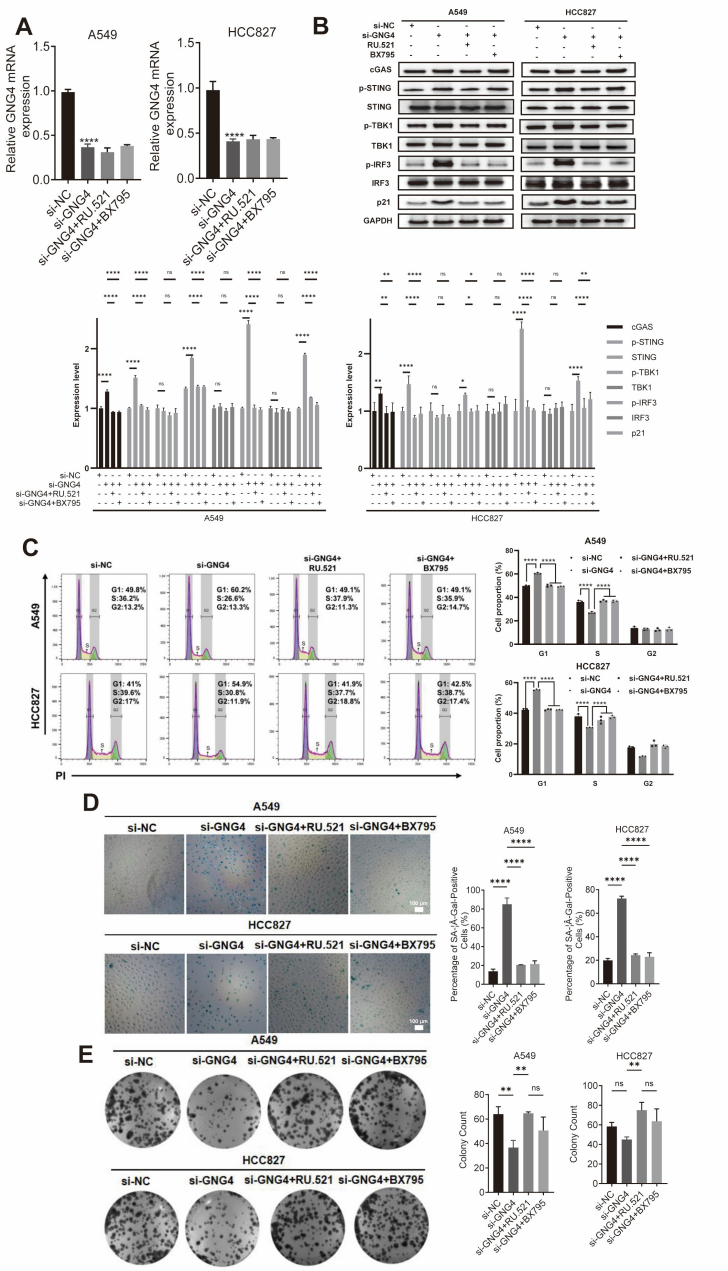

Fig. 2. GNG4 suppresses LUAD cells senescence and promotes its proliferation by downregulating the cGAS-STING Pathway. (A) qRT-PCR analysis of GNG4 mRNA expression in A549 and HCC827 cells following GNG4 knockdown and subsequent rescue with RU.521 or BX795. (B) Western blot analysis of cGAS, p-STING/STING, p-TBK1/TBK1, p-IRF3/IRF3, and p21 protein expression in A549 and HCC827 cells following GNG4 knockdown and subsequent rescue with RU.521 or BX795. (C) Flow cytometry analysis of cell cycle distribution in A549 and HCC827 cells following GNG4 knockdown and subsequent rescue with RU.521 or BX795. (D) SA-β-Gal staining assessing cellular senescence in A549 and HCC827 cells following GNG4 knockdown and subsequent rescue with RU.521 or BX795. (E) Colony formation assay evaluating proliferative capacity in A549 and HCC827 cells following GNG4 knockdown and subsequent rescue with RU.521 or BX795. mRNA and protein levels are expressed as fold change relative to the vehicle control after normalization to GAPDH. TBK1, TANK-binding kinase 1; IRF3, Interferon regulatory factor 3. $p < 0.05$ was considered statistically significant. ns, non-significant, *$p < 0.05$, **$p < 0.01$, ****$p < 0.0001$.

protein IGF2BP3 (Fig. 3I). These findings suggested that the elevated expression of GNG4 in LUAD may be post-transcriptionally regulated by m6A methylation and closely associated with the functions of VIRMA and IGF2BP3.

VIRMA Promotes m6A Methylation of GNG4 to Enhance Its mRNA Expression

To elucidate the regulatory roles of VIRMA in m6A methylation and mRNA expression of GNG4, we knocked

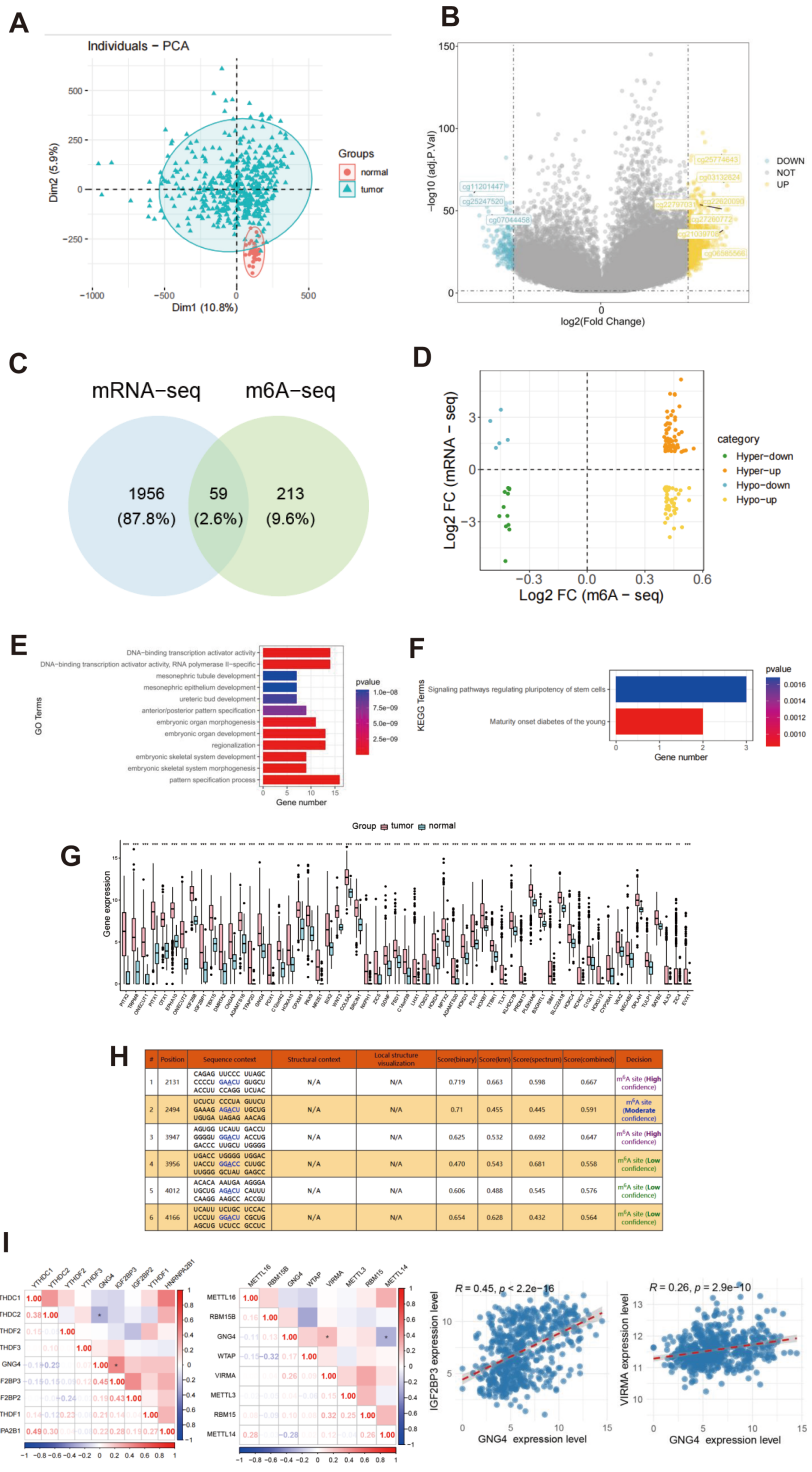

Fig. 3. Increased m6A methylation promotes mRNA expression of GNG4 in LUAD. (A) PCA of m6A methylation profiles in LUAD. (B) Volcano plot of differentially methylated genes in LUAD. (C) Venn diagram showing 59 genes consistently upregulated at both the methylation and transcriptional levels in tumor samples. (D) Scatter plot displaying the distribution of co-upregulated genes based on logFC values from methylation and transcriptome datasets. (E) GO enrichment analysis of the 59 overlapping genes. (F) KEGG pathway enrichment analysis of the 59 overlapping genes. (G) Box plot illustrating expression levels of the 59 overlapping genes. (H) Predicted m6A methylation sites in GNG4 mRNA by SRAMP analysis. (I) Correlation heatmap and scatter plots depicting associations between GNG4 expression and m6A writers/readers. m6A, N6-methyladenosine; PCA, principal component analysis; GO, Gene Ontology; KEGG, Kyoto Encyclopedia of Genes and Genomes; SRAMP, sequence-based RNA adenosine methylation site predictor. *$p < 0.05$, **$p < 0.01$, ***$p < 0.001$.

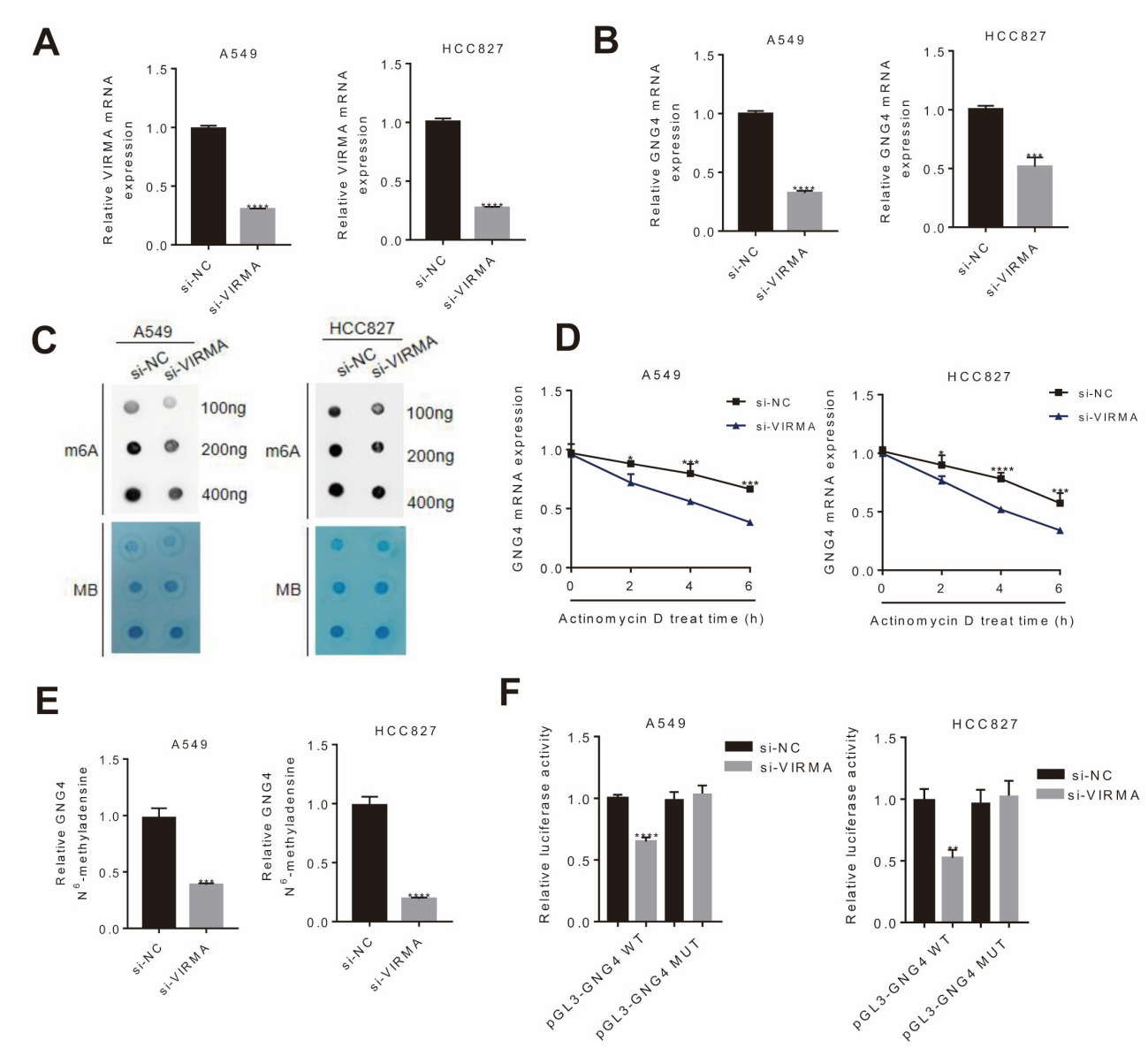

Fig. 4. VIRMA promotes m6A methylation of GNG4 to enhance its mRNA expression. (A) qRT-PCR analysis of VIRMA mRNA expression in A549 and HCC827 cells following VIRMA knockdown. (B) qRT-PCR analysis of GNG4 mRNA expression in A549 and HCC827 cells following VIRMA knockdown. (C) m6A dot blot assay-detected changes in m6A methylation levels in A549 and HCC827 cells following VIRMA knockdown. (D) qRT-PCR analysis of GNG4 mRNA half-life in A549 and HCC827 cells after VIRMA knockdown and actinomycin D treatment. (E) MeRIP-qPCR validation of GNG4 m6A methylation levels in A549 and HCC827 cells following VIRMA knockdown. (F) Dual-luciferase reporter assay comparing luciferase activity between wild-type and mutant reporter constructs in A549 and HCC827 cells following VIRMA knockdown. mRNA levels are expressed as fold change relative to the vehicle control after normalization to GAPDH. VIRMA, Vir like m6A methyltransferase associated. *$p < 0.05$ vs. si-NC group; *$p < 0.05$ vs. si-NC (pGL3-GNG4 WT) group in (F); $p < 0.05$ was considered statistically significant. **$p < 0.01$, ***$p < 0.001$, ****$p < 0.0001$.

down VIRMA in LUAD cell lines A549 and HCC827. Knockdown of VIRMA (Fig. 4A, $p < 0.0001$) significantly reduced both the mRNA expression and stability of GNG4 (Fig. 4B,D; $p < 0.05$). m6A dot blot assays further demonstrated that depletion of VIRMA markedly decreased the m6A methylation level of A549 and HCC817 (Fig. 4C), MeRIP-qPCR further demonstrated that knocking down VIRMA significantly reduced the m6A level of GNG4 in both A549 and HCC827 cells (Fig. 4E, $p < 0.001$). To investigate the m6A regulation of GNG4 at site 2131 (A) by VIRMA, we constructed two reporter plasmids: a wild-type (GNG4 WT) plasmid and a mutant (GNG4 MUT) plasmid. These were generated by inserting sequences containing either the wild-type GNG4 site 2131 with its flanking regions (typically several hundred base pairs) or a mutant version (A-to-T substitution) with its flanking regions into

the 3'UTR of the Renilla luciferase gene. Following transfection with either si-NC (negative control) or si-VIRMA, the relative m6A-dependent regulatory effect mediated by VIRMA was assessed by comparing the luciferase activity between the GNG4 WT and GNG4 MUT reporter plasmids. We observed that the fluorescence intensity of the GNG4 MUT reporter plasmid was significantly weaker than that of the GNG4 WT plasmid. Furthermore, knocking down VIRMA markedly reduced the fluorescence intensity of the GNG4 WT plasmid (Fig. 4F, $p < 0.01$), indicating that VIRMA exerted its regulatory function through m6A modification of the adenosine at site 2131 in GNG4.

IGF2BP3 Facilitates the Expression of GNG4 mRNA by Recognizing and Stabilizing Its m6A Modifications

Similarly, knockdown of IGF2BP3 (Fig. 5A, $p < 0.0001$) led to consistent and significant reductions in GNG4 mRNA expression, stability (Fig. 5B,C; $p < 0.05$), and m6A methylation levels (Fig. 5D, $p < 0.05$), indicating that IGF2BP3, as an m6A reader, participated in the post-transcriptional regulation of GNG4. Furthermore, RNA pulldown assays showed that GNG4 mRNA specifically binds to IGF2BP3 protein (Fig. 5E), providing molecular evidence for the direct recognition and regulation of GNG4 by IGF2BP3.

VIRMA Promotes LUAD Progression by Stabilizing GNG4 mRNA to Inhibit the cGAS-STING Pathway

To determine whether the regulatory effect of GNG4 on the cGAS-STING pathway depended on its m6A methylation, we performed rescue experiments in LUAD cells: following knockdown of the m6A methyltransferase VIRMA, we reintroduced a GNG4 overexpression plasmid (Fig. 6A–C, $p < 0.001$). Results showed that VIRMA knockdown significantly reduced the m6A methylation level of GNG4, which could not be restored by GNG4 overexpression (Fig. 6D, $p < 0.0001$), confirming that m6A modification of GNG4 was indeed dependent on VIRMA. Functionally, VIRMA knockdown markedly activated the cGAS-STING pathway, as indicated by the increased expression of cGAS, p-STING/STING, p-TBK1/TBK1, p-IRF3/IRF3, and p21 proteins. This activation was effectively suppressed upon GNG4 overexpression (Fig. 6E). Phenotypically, flow cytometry (Fig. 6G, $p < 0.0001$), EdU staining (Fig. 6I, $p < 0.05$), and CCK-8 assays (Fig. 6J, $p < 0.001$) consistently indicated that VIRMA knockdown suppressed LUAD cell proliferation, while GNG4 overexpression restored proliferative capacity. Meanwhile, senescence-associated analyses revealed that VIRMA knockdown enhanced SA-β-Gal staining (Fig. 6F, $p < 0.0001$) and increased secretion of SASP factors (Fig. 6H, $p < 0.001$), whereas GNG4 overexpression significantly attenuated cellular senescence ($p < 0.001$). Together, these findings demonstrated that GNG4 negatively regulated the cGAS-STING pathway in an m6A-dependent manner, thereby inhibiting cellular senescence and promoting proliferation in LUAD.

VIRMA Mediated m6A Modification of GNG4 Promotes LUAD Progression by Inhibiting the cGAS-STING Pathway

In order to further confirm the regulatory function of GNG4 on the cGAS-STING pathway in LUAD progression and the regulatory mechanism of VIRMA-mediated m6A modification on GNG4 *in vivo*, we employed a mouse subcutaneous xenograft tumor model for validation. The results demonstrated that knocking down GNG4 significantly up-regulated the expression of core proteins in the cGAS-STING pathway in tumor tissues (Fig. 7A), indicating *in vivo* activation of this pathway. Meanwhile, after evaluating the knockdown efficiency of GNG4 and VIRMA (Fig. 7B, $p < 0.001$), it was found that knockdown of VIRMA led to a significant reduction in both the mRNA expression level (Fig. 7C, $p < 0.001$) and the m6A modification level of GNG4 (Fig. 7D, $p < 0.001$). Concurrently, measurements of tumor volume and weight demonstrated that tumor growth was markedly suppressed in the GNG4- and VIRMA-knockdown group, with significantly smaller tumors observed (Fig. 7E, $p < 0.0001$). Assessment of tumor sections by immunohistochemistry revealed that knockdown of GNG4 or VIRMA *in vivo* reduced the abundance of key proliferative markers (Ki-67, PCNA, PHH3). Conversely, a significant increase in SA-β-Gal, a marker associated with cellular senescence, was observed under the same conditions (Fig. 7F, $p < 0.001$). Furthermore, changes in the levels of tumor markers (TK1, CEA, AFP) and SASP factors in mouse serum were consistent with these findings (Fig. 7G,H; $p < 0.0001$), further supporting the conclusion that GNG4 and VIRMA knockdown inhibited tumor proliferation and promoted senescence. These *in vivo* results demonstrated that VIRMA–mediated m6A modification of GNG4 played a critical regulatory role in LUAD progression by suppressing the cGAS-STING signaling pathway.

Discussion

This research offers a detailed investigation into the regulatory mechanisms of m6A methylation in LUAD. Importantly, it reveals for the first time that the G protein subunit GNG4, acting as a critical target of m6A modification, promotes LUAD cell proliferation by inhibiting the cGAS-STING signaling pathway.

As a central hub in the tumor microenvironment, the cGAS-STING pathway triggers cellular senescence in tumor cells and further modulates the trajectory of tumor development. For example, the traditional Chinese medication Bazi BuShen can enhance immune clearance of senescent liver cancer cells via cGAS–STING activation in

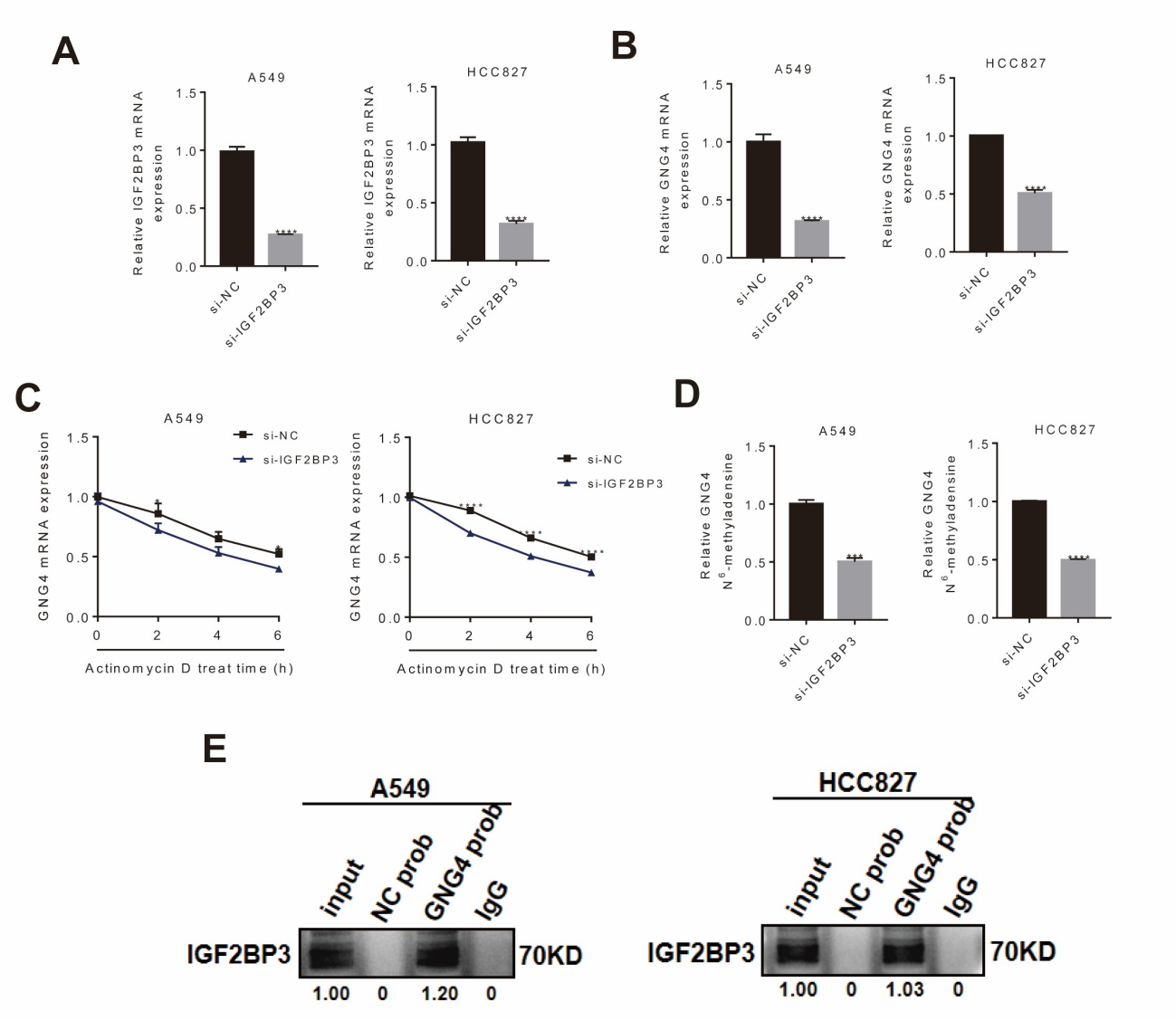

Fig. 5. IGF2BP3 facilitates the expression of GNG4 mRNA by recognizing and stabilizing its m6A modifications. (A) qRT-PCR analysis of IGF2BP3 mRNA expression in A549 and HCC827 cells following IGF2BP3 knockdown. (B) qRT-PCR measurement of GNG4 mRNA expression in A549 and HCC827 cells following IGF2BP3 knockdown. (C) qRT-PCR analysis of GNG4 mRNA half-life in A549 and HCC827 cells after IGF2BP3 knockdown and actinomycin D treatment. (D) MeRIP-qPCR validation of GNG4 m6A methylation levels in A549 and HCC827 cells following IGF2BP3 knockdown. (E) RNA pulldown assay examining the binding interaction between IGF2BP3 and GNG4 mRNA in A549 and HCC827 cells. mRNA levels are expressed as fold change relative to the vehicle control after normalization to GAPDH. *$p < 0.05$ vs. si-NC group; $p < 0.05$ was considered statistically significant. ***$p < 0.001$, ****$p < 0.0001$.

macrophages [26]. Oroxylin A regulates this pathway to activate ferritinophagy and induce hepatic stellate cell senescence, thereby counteracting liver fibrosis [27]. Similarly, the cGAS-STING pathway has been confirmed as a key participant in lung adenocarcinoma: TET2 inhibits LUAD cell proliferation and metastasis by activating this pathway [28], while ESYT3 overexpression enhances cGAS-STING activity and improves radiotherapeutic response in LUAD [29]. Moreover, multiple studies have confirmed that activation of cGAS-STING pathway-related genes is significantly associated with better prognosis in LUAD patients [30], highlighting its clinical importance. Based on prior research, this work further clarified the crucial function of the m6A modification—GNG4—cGAS/STING regulatory axis in the development of LUAD, providing new experimental evidence for the underlying mechanism and potential targeted therapies.

VIRMA and IGF2BP3, the key “writer” and “reader” of m6A methylation, are highly expressed in various cancers including LUAD and significantly promote tumor pro-

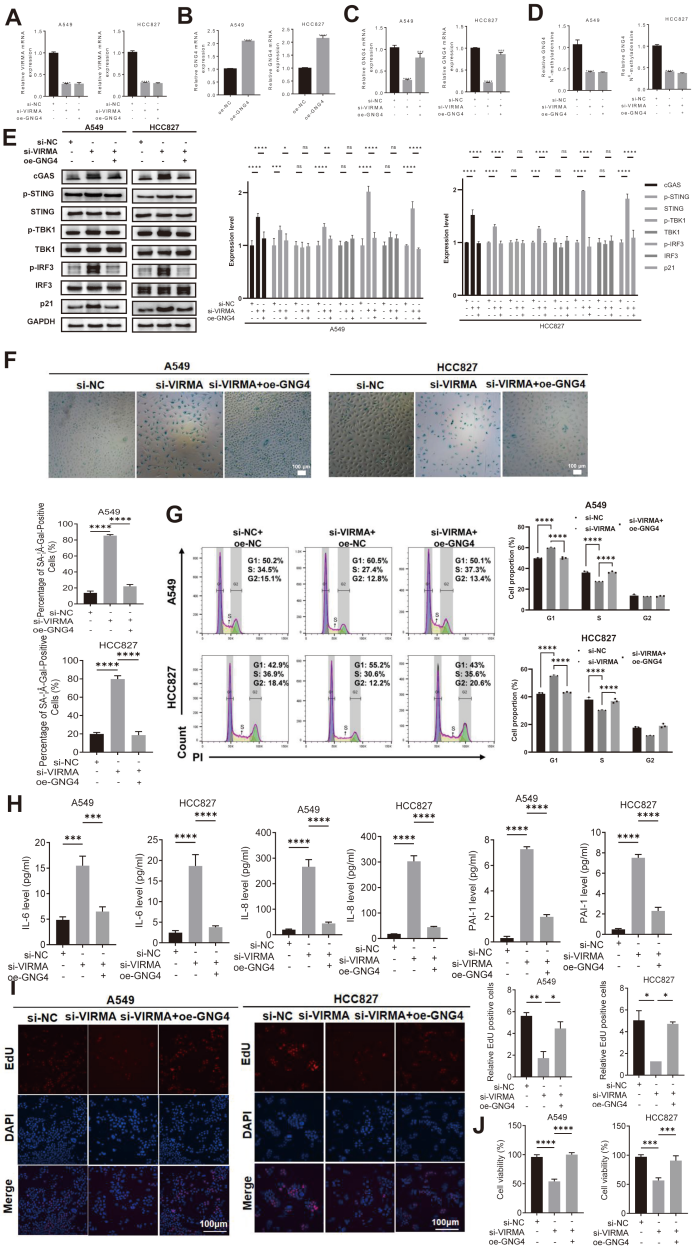

Fig. 6. VIRMA promotes LUAD progression by stabilizing GNG4 mRNA to inhibit the cGAS-STING pathway. (A) qRT-PCR analysis of VIRMA mRNA expression in A549 and HCC827 cells after VIRMA knockdown followed by GNG4 overexpression. (B) qRT-PCR analysis of GNG4 mRNA expression in A549 and HCC827 cells after GNG4 overexpression. (C) qRT-PCR measurement of GNG4 mRNA expression in A549 and HCC827 cells after VIRMA knockdown followed by GNG4 overexpression. (D) MeRIP-qPCR detection of m6A methylation levels on GNG4 mRNA in A549 and HCC827 cells after VIRMA knockdown followed by GNG4 overexpression. (E) Western blot analysis of cGAS, p-STING/STING, p-TBK1/TBK1, p-IRF3/IRF3, and p21 protein expression in A549 and HCC827 cells after VIRMA knockdown followed by GNG4 overexpression. (F) Flow cytometry analysis of cell cycle distribution in A549 and HCC827 cells after VIRMA knockdown followed by GNG4 overexpression. (G) SA-β-Gal staining assessing cellular senescence in A549 and HCC827 cells after VIRMA knockdown followed by GNG4 overexpression. (H) ELISA measurement of IL-6, IL-8, and PAI-1 secretion in A549 and HCC827 cells after VIRMA knockdown followed by GNG4 overexpression. (I) EdU staining detecting proliferative activity in A549 and HCC827 cells after VIRMA knockdown followed by GNG4 overexpression. (J) CCK-8 assay measuring cell viability in A549 and HCC827 cells after VIRMA knockdown followed by GNG4 overexpression. mRNA and protein levels are expressed as fold change relative to the vehicle control after normalization to GAPDH. $^{*}p < 0.05$ vs. si-NC group; $^{\#}p < 0.05$ vs. si-VIRMA group; $p < 0.05$ was considered statistically significant. ns, non-significant, $^{*}p < 0.05$, $^{**}p < 0.01$, $^{***}p < 0.001$, $^{****}p < 0.0001$, $^{\#\#\#}p < 0.001$.

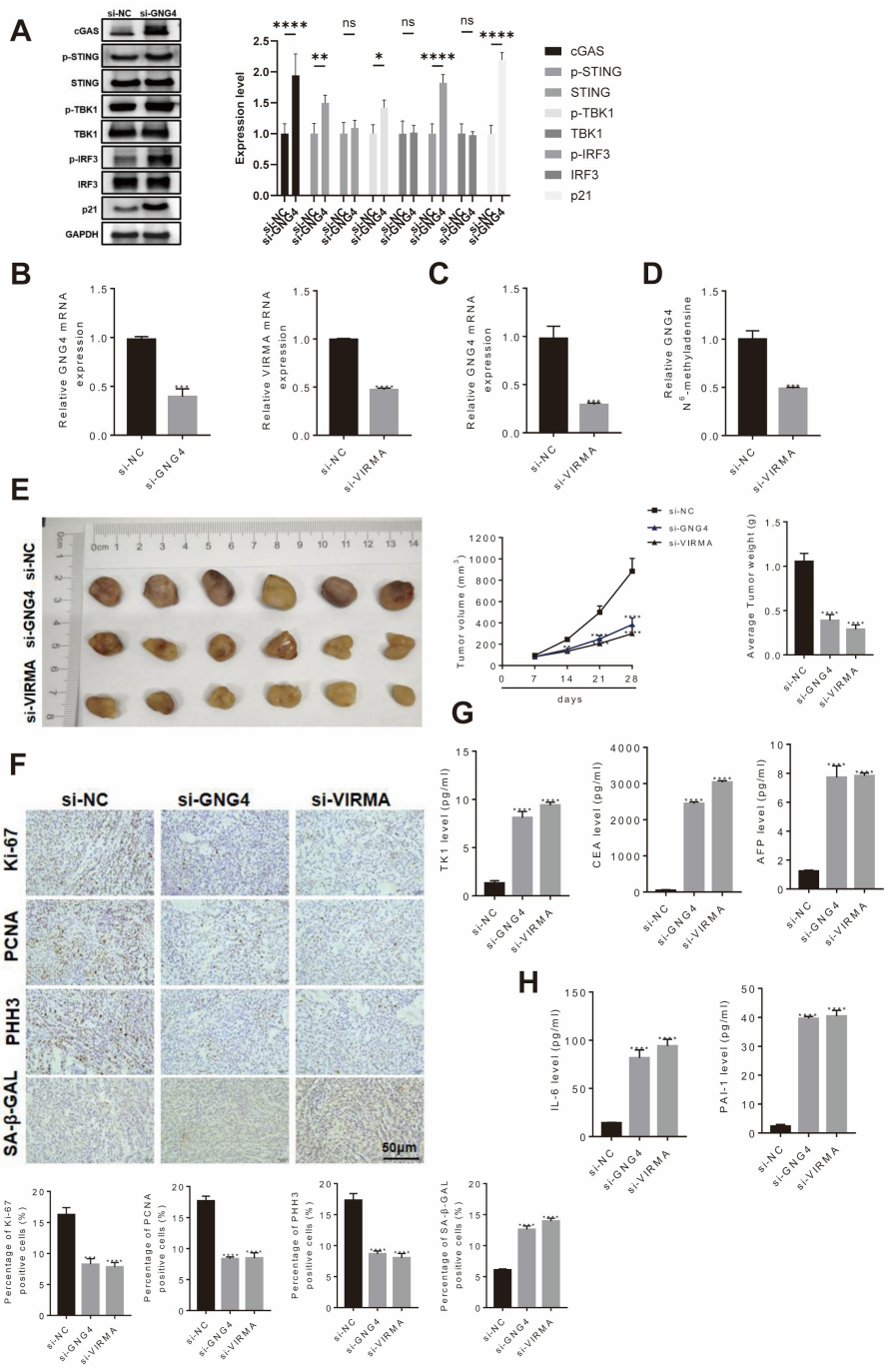

Fig. 7. VIRMA-mediated m6A modification of GNG4 promotes LUAD progression by inhibiting the cGAS-STING Pathway. (A) Western blot analysis of cGAS, p-STING/STING, p-TBK1/TBK1, p-IRF3/IRF3, and p21 protein expression in tumor tissues after GNG4 knockdown. (B) qRT-PCR measurement of GNG4 or VIRMA mRNA expression in tumor tissues after GNG4 or VIRMA knockdown. (C) qRT-PCR measurement of GNG4 mRNA expression in tumor tissues after VIRMA knockdown. (D) MeRIP-qPCR detection of m6A methylation levels in GNG4 mRNA in tumor tissues after VIRMA knockdown. (E) Measurement of tumor volume and weight changes following GNG4 and VIRMA knockdown. (F) Immunohistochemical detection of Ki-67, PCNA, PHH3, and SA-β-Gal expression in tumor tissues after GNG4 and VIRMA knockdown. (G) ELISA analysis of serum levels of TK1, CEA, and AFP after GNG4 and VIRMA knockdown. (H) ELISA measurement of serum levels of PAI-1, and IL-6 following GNG4 and VIRMA knockdown. mRNA and protein levels are expressed as fold change relative to the vehicle control after normalization to GAPDH. *$p < 0.05$ vs. si-NC group; $p < 0.05$ was considered statistically significant. ns, non-significant, *$p < 0.05$, **$p < 0.01$, ***$p < 0.001$, ****$p < 0.0001$.

gression. Studies have shown that VIRMA, an RNA methyltransferase driven by gene amplification, regulates BTG2 expression in an m6A-YTHDF2-dependent manner to facilitate LUAD tumorigenesis [31]. VIRMA also enhances the cytoplasmic stability of HAS2 through an m6A-dependent mechanism, accelerating breast cancer progression [32]. On the other hand, through m6A modification, IGF2BP3 modulates TFAP2A activity, leading to the transcriptional upregulation of SLC7A11/GPX4 and a consequent inhibition of ferroptosis in LUAD [33]. These findings underscore the crucial role of VIRMA- and IGF2BP3-mediated m6A modification in cancer development. Extending previous work, our study innovatively demonstrated the important role of VIRMA and IGF2BP3 in LUAD progression through m6A-dependent regulation of GNG4, offering novel mechanistic insights and future research directions for m6A applications in LUAD.

Our findings established GNG4 as a crucial functional target of m6A modification. We verified through bioinformatics analysis and subsequent experiments that GNG4 exhibits significant upregulation in LUAD. Its elevated expression is strongly and positively correlated with the levels of the m6A methyltransferase VIRMA and the m6A-binding protein IGF2BP3. This result not only expanded the target gene spectrum of the m6A regulatory network but, more importantly, mechanistically explains the aberrant overexpression of GNG4 in LUAD: the stability and translation efficiency of its mRNA were likely synergistically enhanced by VIRMA-mediated methylation and IGF2BP3-mediated recognition. Using site-directed mutagenesis and dual-luciferase reporter assays, we further confirmed the functional importance of its specific m6A modification site, providing direct molecular evidence for epitranscriptomic regulation.

The core discovery of our study lied in elucidating the downstream mechanisms and biological effects of GNG4. GSEA enrichment analysis and subsequent functional experiments collectively demonstrated that loss of GNG4 significantly activated the cGAS-STING signaling pathway, triggering irreversible cell cycle arrest and a senescent phenotype, ultimately inhibiting tumor proliferation. This finding had multiple implications: first, it connected G protein signaling and innate immune signaling—two pathways critical in cancer—revealing a new strategy by which tumor cells suppressed innate immune surveillance through epitranscriptomic regulation; second, it identified cellular senescence as a key terminal effect following GNG4 inhibition, providing a theoretical basis and potential target for "pro-senescence therapy" in LUAD. Notably, both *in vitro* and *in vivo* experiments confirmed that targeting GNG4 or its upstream regulators VIRMA/IGF2BP3 effectively activated the cGAS–STING pathway and inhibited tumor growth, highlighting the therapeutic potential of this axis. Particularly encouraging are the significant changes in tumor markers and SASP factors observed in animal models, suggesting that therapeutic strategies targeting this pathway may have promising *in vivo* applicability.

Conclusion

The study reveals that upregulated m^6A modification of GNG4 in lung adenocarcinoma (LUAD) enhances its mRNA stability, leading to elevated GNG4 expression. Functionally, increased GNG4 suppresses the cGAS–STING signaling pathway, thereby attenuating the cellular innate immune response to cytosolic DNA and stress signals. The inhibition of the cGAS–STING pathway consequently blocks the initiation of cellular senescence, allowing tumor cells to escape senescence-associated growth arrest. This ultimately promotes LUAD cell proliferation and accelerates tumor progression. Collectively, our findings identify a novel oncogenic axis in LUAD involving m^6A-mediated upregulation of GNG4 and subsequent repression of the cGAS–STING pathway. Targeting the m^6A modification of GNG4 or restoring cGAS–STING activity may represent a promising therapeutic strategy to suppress LUAD progression.

Availability of Data and Materials

The data and materials in the current study are available from the corresponding author on reasonable request.

Author Contributions

JunM, JieM, JHL, XW and YW contributed to the study design. JunM, JHL and XW conducted the literature search. JunM, JieM and YW acquired the data. JunM and JHL wrote the article. XW and YW performed data analysis. JieM, JHL, XW and YW critically revised the article. All authors gave the final approval of the version to be submitted. All authors read and approved the final manuscript. All authors have participated sufficiently in the work to take public responsibility for appropriate portions of the content and agreed to be accountable for all aspects of the work in ensuring that questions related to its accuracy or integrity.

Ethics Approval and Consent to Participate

This study was was approved by the Experimental Animal Ethics Committee of Heji Hospital Affiliated to Changzhi Medical College (DW2026003).

Acknowledgment

Not applicable.

Funding

This research received no external funding.

Conflict of Interest

The authors declare no conflict of interest.

References

[1] Wei X, Li X, Hu S, Cheng J, Cai R. Regulation of Ferroptosis in Lung Adenocarcinoma. International Journal of Molecular Sciences. 2023; 24: 14614. https://doi.org/10.3390/ijms241914614.

[2] Li G, Guo J, Mou Y, Luo Q, Wang X, Xue W, *et al*. Keratin gene signature expression drives epithelial-mesenchymal transition through enhanced TGF-β signaling pathway activation and correlates with adverse prognosis in lung adenocarcinoma. Heliyon. 2024; 10: e24549. https://doi.org/10.1016/j.heliyon.2024.e24549.

[3] Zhao F, Chen M, Wu T, Ji M, Li F. Integration of single-cell and bulk RNA sequencing to identify a distinct tumor stem cells and construct a novel prognostic signature for evaluating prognosis and immunotherapy in LUAD. Journal of Translational Medicine. 2025; 23: 222. https://doi.org/10.1186/s12967-025-06243-6.

[4] Hu W, Yang J, Hu K, Luo G, Chen Z, Lu Z, *et al*. Identification of TEFM as a potential therapeutic target for LUAD treatment. Journal of Translational Medicine. 2024; 22: 692. https://doi.org/10.1186/s12967-024-05483-2.

[5] Liu Y, Yu M, Cheng X, Zhang X, Luo Q, Liao S, *et al*. A novel LUAD prognosis prediction model based on immune checkpoint-related lncRNAs. Frontiers in Genetics. 2022; 13: 1016449. https://doi.org/10.3389/fgene.2022.1016449.

[6] Jin J, Liu C, Yu S, Cai L, Sitrakiniaina A, Gu R, *et al*. A novel ferroptosis-related gene signature for prognostic prediction of patients with lung adenocarcinoma. Aging. 2021; 13: 16144–16164. https://doi.org/10.18632/aging.203140.

[7] Zaccara S, Ries RJ, Jaffrey SR. Publisher Correction: Reading, writing and erasing mRNA methylation. Nature Reviews. Molecular Cell Biology. 2023; 24: 770. https://doi.org/10.1038/s41580-023-00654-3.

[8] Li F, Wang H, Huang H, Zhang L, Wang D, Wan Y. m6A RNA Methylation Regulators Participate in the Malignant Progression and Have Clinical Prognostic Value in Lung Adenocarcinoma. Frontiers in Genetics. 2020; 11: 994. https://doi.org/10.3389/fgene.2020.00994.

[9] Wang S, Gu X, Xu D, Liu B, Qin K, Yuan X. Comprehensive analysis of m6A modification patterns and m6A-related lncRNAs as potential biomarkers in lung adenocarcinoma. Environmental Toxicology. 2024; 39: 2285–2303. https://doi.org/10.1002/tox.24110.

[10] Yang S, Li K, Zhang J, Liu J, Liu L, Tan Y, *et al*. Link between m6A modification and infiltration characterization of tumor microenvironment in lung adenocarcinoma. Experimental Biology and Medicine. 2023; 248: 2273–2288. https://doi.org/10.1177/15353702231214266.

[11] Liu J, Li Z, Cheang I, Li J, Zhou C. RNA-Binding Protein IGF2BP1 Associated With Prognosis and Immunotherapy Response in Lung Adenocarcinoma. Frontiers in Genetics. 2022; 13: 777399. https://doi.org/10.3389/fgene.2022.777399.

[12] Liang L, Huang J, Yao M, Li L, Jin XJ, Cai XY. GNG4 Promotes Tumor Progression in Colorectal Cancer. Journal of Oncology. 2021; 2021: 9931984. https://doi.org/10.1155/2021/9931984.

[13] Tanaka H, Kanda M, Miwa T, Umeda S, Sawaki K, Tanaka C, *et al*. G-protein subunit gamma-4 expression has potential for detection, prediction and therapeutic targeting in liver metastasis of gastric cancer. British Journal of Cancer. 2021; 125: 220–228. https://doi.org/10.1038/s41416-021-01366-1.

[14] Jiang X, Tang F, Zhang J, He M, Xie T, Tang H, *et al*. High GNG4 predicts adverse prognosis for osteosarcoma: Bioinformatics prediction and experimental verification. Frontiers in Oncology. 2023; 13: 991483. https://doi.org/10.3389/fonc.2023.991483.

[15] Zhao H, Sheng D, Qian Z, Ye S, Chen J, Tang Z. Identifying GNG4 might play an important role in colorectal cancer TMB. Cancer Biomarkers. 2021; 32: 435–450. https://doi.org/10.3233/CBM-203009.

[16] Zhou B, Zhu W, Yuan S, Wang Y, Zhang Q, Zheng H, *et al*. High GNG4 expression is associated with poor prognosis in patients with lung adenocarcinoma. Thoracic Cancer. 2022; 13: 369–379. https://doi.org/10.1111/1759-7714.14265.

[17] Gao Z, Yang J. GNB4 Silencing Promotes Pyroptosis to Inhibit the Development of Glioma by Activating cGAS-STING Pathway. Mol Biotechnol. 2025; 67: 2262–2276. https://doi.org/10.1007/s12033-024-01194-7.

[18] Sprang SR. G protein mechanisms: insights from structural analysis. Annual Review of Biochemistry. 1997; 66: 639–678. https://doi.org/10.1146/annurev.biochem.66.1.639.

[19] Chung YK, Wong YH. Re-examining the 'Dissociation Model' of G protein activation from the perspective of G$\beta\gamma$ signaling. The FEBS Journal. 2021; 288: 2490–2501. https://doi.org/10.1111/febs.15605.

[20] Bonham LW, Evans DS, Liu Y, Cummings SR, Yaffe K, Yokoyama JS. Neurotransmitter Pathway Genes in Cognitive Decline During Aging: Evidence for GNG4 and KCNQ2 Genes. American Journal of Alzheimer's Disease and other Dementias. 2018; 33: 153–165. https://doi.org/10.1177/1533317517739384.

[21] Yang H, Wang H, Ren J, Chen Q, Chen ZJ. cGAS is essential for cellular senescence. Proceedings of the National Academy of Sciences of the United States of America. 2017; 114: E4612–E4620. https://doi.org/10.1073/pnas.1705499114.

[22] Criscione SW, Teo YV, Neretti N. The Chromatin Landscape of Cellular Senescence. Trends in Genetics. 2016; 32: 751–761. https://doi.org/10.1016/j.tig.2016.09.005.

[23] Frediani E, Scavone F, Laurenzana A, Chillà A, Tortora K, Cimmino I, *et al*. Olive phenols preserve lamin B1 expression reducing cGAS/STING/NFκB-mediated SASP in ionizing radiation-induced senescence. Journal of Cellular and Molecular Medicine. 2022; 26: 2337–2350. https://doi.org/10.1111/jcmm.17255.

[24] Wang L, Guo J, Lv C, Kong L, Cui J, Wang Z, *et al*. MiR-145-5p arrests the cell cycle by modulating SMAD5/cyclin D1 to inhibit gastric cancer progression. Frontiers in Cell and Developmental Biology. 2025; 13: 1619359. https://doi.org/10.3389/fcell.2025.1619359.

[25] Zhao H, Cao N, Liu Q, Zhang Y, Jin R, Lai H, *et al*. Inhibition of the E3 ligase UBR5 stabilizes TERT and protects vascular organoids from oxidative stress. Journal of Translational Medicine. 2024; 22: 1080. https://doi.org/10.1186/s12967-024-05887-0.

[26] Xing F, Lv H, Xiang W, Wang L, Zong Q, Lv G, *et al*. Traditional medicine Bazi Bushen potentiates immunosurveillance of senescent liver cancer cells via cGAS-STING signaling activation in macrophages. Cancer Letters. 2025; 627: 217544. https://doi.org/10.1016/j.canlet.2025.217544.

[27] Sun Y, Weng J, Chen X, Ma S, Zhang Y, Zhang F, *et al*. Oroxylin A activates ferritinophagy to induce hepatic stellate cell senescence against hepatic fibrosis by regulating cGAS-STING pathway. Biomedicine & Pharmacotherapy. 2023; 162: 114653. https://doi.org/10.1016/j.biopha.2023.114653.

[28] Cheng G, Wu J, Ji M, Hu W, Wu C, Jiang J. TET2 inhibits the proliferation and metastasis of lung adenocarcinoma cells via activation of the cGAS-STING signalling pathway. BMC Cancer. 2023; 23: 825. https://doi.org/10.1186/s12885-023-11343-x.

[29] Luo Z, Li Y, Xu B, Yu T, Luo M, You P, *et al*. Overexpression of ESYT3 improves radioimmune responses through activating cGAS-STING pathway in lung adenocarcinoma. Experimental Hematology & Oncology. 2024; 13: 77. https://doi.org/10.1186/s40164-024-00546-y.

[30] Huang X, Lv X, Cao X. Identification of Prognosis Signature Based on cGAS-STING Pathway and Its Immunotherapeutic Significance in Lung Adenocarcinoma. Molecular Biotechnology. 2026; 68: 308–322. https://doi.org/10.1007/s12033-025-01376-x.

[31] Zhang C, Sun Q, Zhang X, Qin N, Pu Z, Gu Y, *et al*. Gene amplification-driven RNA methyltransferase KIAA1429 promotes tumorigenesis by regulating BTG2 via m6A-YTHDF2-dependent in lung adenocarcinoma. Cancer Communications. 2022; 42: 609–626. https://doi.org/10.1002/cac2.12325.

[32] Li N, Zhu Z, Deng Y, Tang R, Hui H, Kang Y, *et al*. KIAA1429/VIRMA promotes breast cancer progression by m^6A-dependent cytosolic HAS2 stabilization. EMBO Reports. 2023; 24: e55506. https://doi.org/10.15252/embr.202255506.

[33] Li P, Chu D, Ding G, Qin D, Bu Y, Tian B. IGF2BP3 suppresses ferroptosis in lung adenocarcinoma by m6A-dependent regulation of TFAP2A to transcriptionally activate SLC7A11/GPX4. Molecular and Cellular Biochemistry. 2025; 480: 2361–2375. https://doi.org/10.1007/s11010-024-05068-z.